Geo-Marine Letters (1995) 15: 1–8

J. Rey · L. Somoza · J. Martínez-Frías

Tectonic, volcanic, and hydrothermal event sequence on Deception Island (Antarctica)

Received: 8 June 1993 / Revision received: 23 May 1994

Abstract On the basis of the correlation between seismic tectonostratigraphic units, volcanism, and geochemical distribution patterns of sea-floor sediments on Deception Island (Antarctica), a regional tectonic extension is suggested to explain the sequence of volcanic and hydrothermal events. The syncollapse caldera episode is composed of five tectonostratigraphic units separated by progressively tilted and bent unconformities. Each unit shows a sequence of Quaternary volcanic cones and mound structures that display high contents of Fe, Mn, and Zn. As-rich active fumaroles and hot-spring areas are associated with the postcollapse episode and linked to normal faulting and present volcanism.

Introduction

Deception Island (DI) shows the most recent active volcanism of the South Shetland Islands (SSI) (Antarctica). The SSI are separated from the Antarctic Peninsula by the Brandsfield Strait (Fig. 1). Tectonically, the DI is located in the confluence zone of two major tectonic structures: the southwestern end of Brandsfield Trough (BT) and the southern prolongation of the Hero Fracture zone. The DI is a ring-shaped volcanic island (Fig. 2), with a flooded caldera that forms a large central bay (Port Foster) that is open to the sea at only one place (Neptune Bellows). Traditionally, this flooded caldera is thought to be a consequence of a catastrophic collapse and subsequent sinking of the major volcanic edifice. Recent volcanic eruptions on DI have been reported in 1967, 1969, and 1970, and continuous earthquake activity also occurs around and on the island.

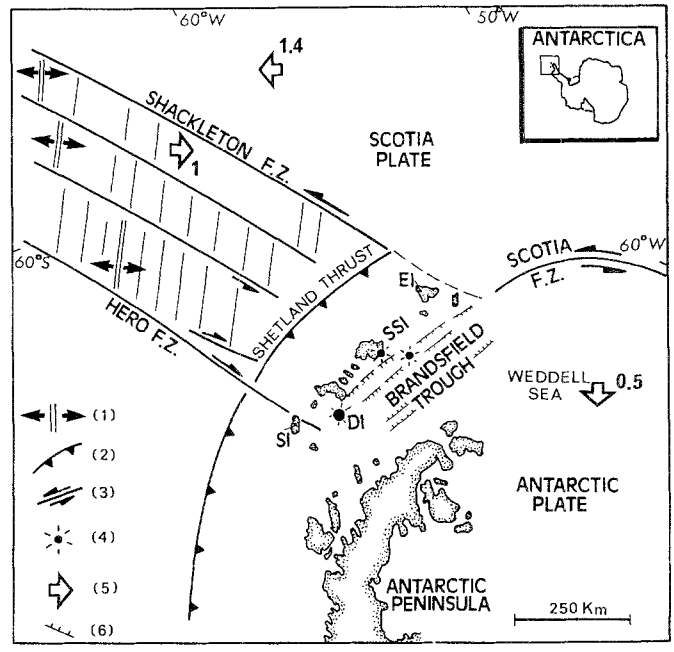

Fig. 1 Regional tectonic framework of the South Shetland Islands (SSI) (DI: Deception Island, SI: Smith Island, EI: Elephant Island) and the Antarctic Peninsula. Legend: (1) oceanic extension ridges; (2) subduction zones (Shetland Thrust); (3) major transcurrent zones: Hero and Shackleton fracture zones; (4) historical volcanoes; (5) relative plate motion (in cm/yr) (after Minster and Jordan 1978); (6) Brandsfield Through

The regional setting of the complex tectonic and volcanic episodes of the SSI has been studied by several authors (Hawkes 1962; Barker et al. 1975; Grad et al. 1992; among others). It is accepted that progressive subduction (that began in the Neogene) of the Drake Plate beneath the Antarctic Plate (Shetland Thrust) has formed the Brandsfield Rift as a consequence of an interarc spreading process (Fig. 1) Synce Early Tertiary times, arc magmatism appears to have diminished all along the Antarctic Peninsula as a

J. Rey (✉)
Instituto Español de Oceanografía, Fuengirola (Málaga), Apto 285, 29640 Spain

L. Somoza
Departamento de Geología, Universidad de Salamanca, Spain

J. Martínez-Frías
Departamento de Geología, Museo Nacional de Ciencias Naturales (CSIC), Madrid, Spain

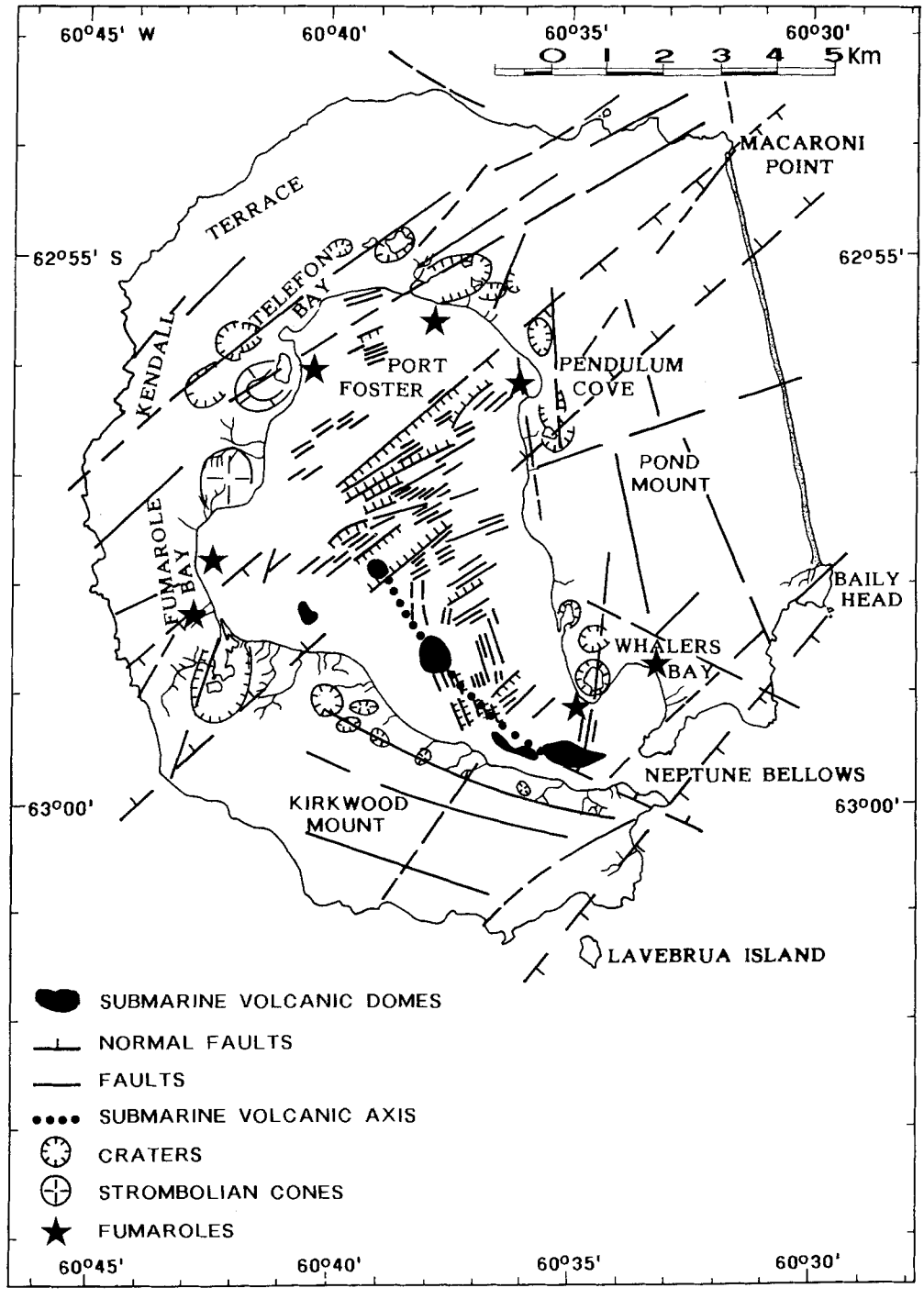

Fig. 2 Fault system and position of the volcanic cones and fumarole areas of Deception Island

result of ridge-crest trench collision (Barker 1982). Smellie (1988) proposed that the arc magmatism in the SSI (and in the Antarctic Peninsula) stopped 4 million yr BP. However, present tectonic processes that strongly affect the area of BT, with recent volcanic and hydrothermal activity at DI, cannot be explained, in our opinion, by a simple model of arc magmatism.

On the basis of both high-resolution seismic profiles and geochemical studies of submarine volcanic sediments, this paper describes the relationship between recent fault systems and submarine volcanic and hydrothermal events. In addition, an alternative geodynamic model is proposed to explain the present location and the features of recent tectonics and volcanism, as they differ from those of the interarc spreading setting.

Submarine and subaerial fault systems

Subaerial faults of the DI show three main systems controlling the geomorphology of the island (Fig. 2). The first

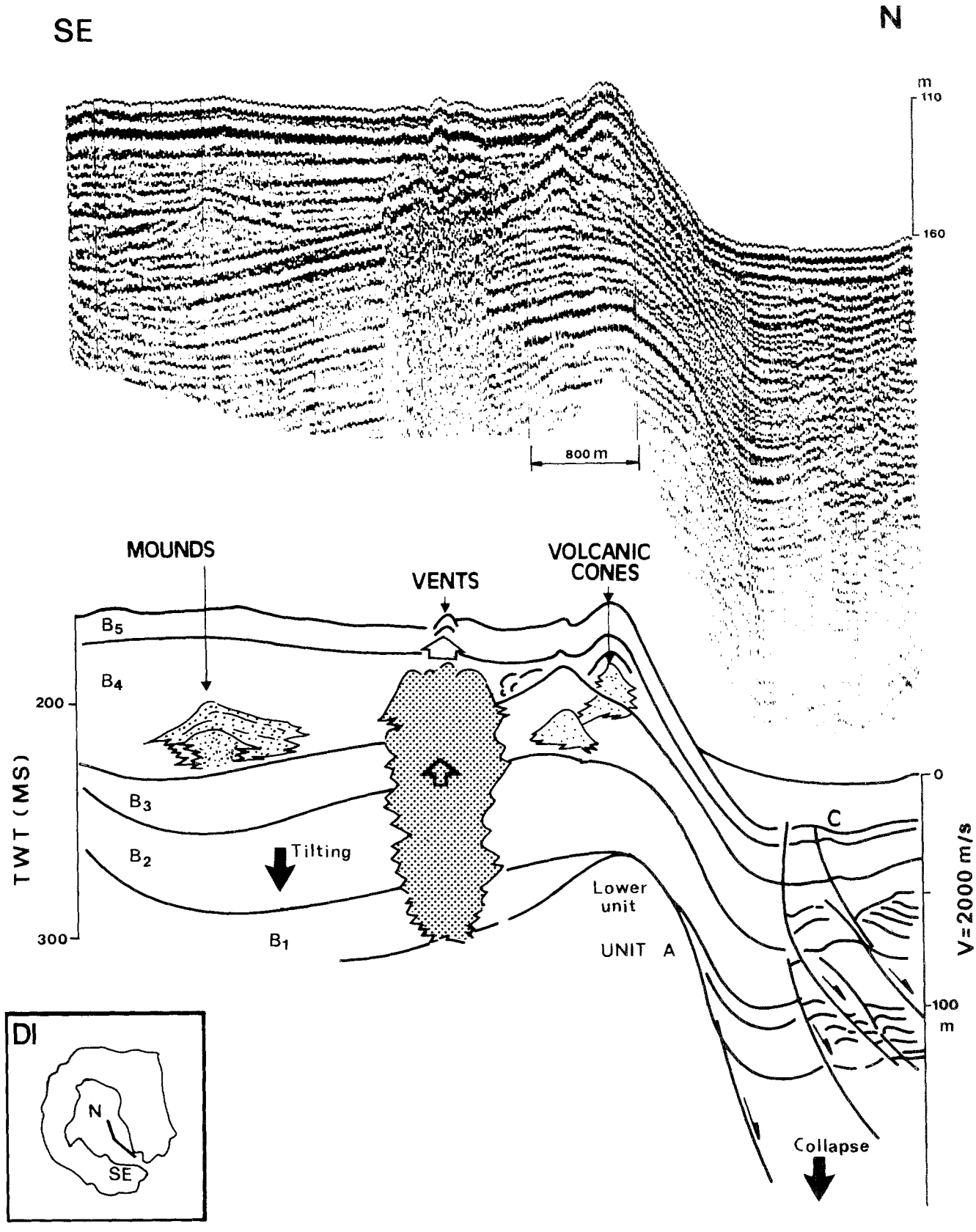

Fig. 3 Seismic reflection profile (Sparker 4000 J) carried out on Deception Island

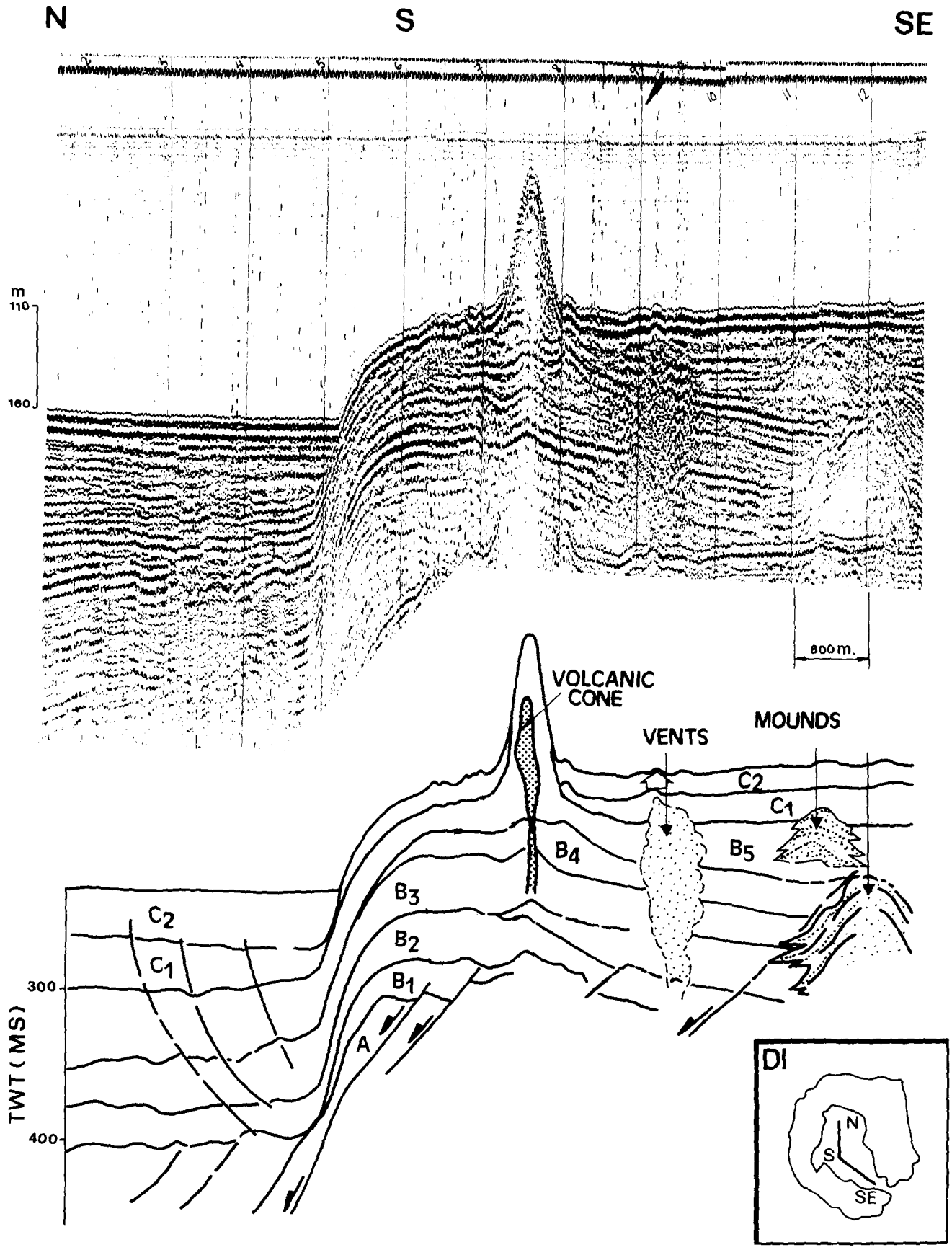

Fig. 4 Seismic reflection profile (Sparker 4000 J) carried out on Deception Island

system strikes from N170 on the east (Macaroni fault) to N160 on the west, near Fumarole Bay. It is responsible for the shape of the coast at Kendall Terrace and Telefon Bay volcanic crater areas (eruptions of 1967 and 1970). This system also controls the shape of the east border of the internal bay, between Pendulum Cove and Whalers Bay. The second system strikes from N60 on the north to N45 on the south. The N45 faults control the shape of DI between La Vebrua Island and Baily Head. Finally, the third system is located around Mount Kirwood and strikes from N115 to N120. It is associated with a cluster of volcanic craters bordering the bay.

Mapping of submarine fault systems from a dense net of seismic profiles (Rey et al. 1990) verifies the prolongation of the N60 faults across the interior of the bay (Fig. 2). Normal faults cause the deepest zones of the bay (up to 160 m), by bending and sinking of volcanic sediment beds located northwards of the line between Pendulum Cove and the southern part of Fumarole Bay (Figs. 3 and 4). Fumarole activity on Fumarole Bay, Pendulum Cove, and Telefon Bay (Fig. 2) appears to be related to this strike (Ortíz et al. 1987). The N170–N160 fault system is poorly defined on the seismic profiles, and it is only located to the south of the major bending structures (Fig. 2).

A submarine volcanic axis composed of several volcanic cones, which strike N150 and are morphologically well preserved (Fig. 4), is observed in the interior of the DI (Fig. 2).

Volcanic events

Subaerial volcanic events of DI have been described by several authors (Barker et al. 1975; González-Ferrán 1985; Smellie 1988). Diverse petrological types and volcanic suites were defined (basalts, basaltic mugearites, andesitic benmoreites, and dacites/trachytes). Recently, Birkenmajer (1992) proposed a new lithostratigraphic pattern to describe the subaerial Quaternary volcanic sequence at DI. This author divides the deposits into the older Foster Group (precaldera deposits) and the younger Hawkes Group, seven formations that include both syncaldera and postcaldera volcanic deposits and cones (Table 1). The Hawkes Group consists of andesitic lapilli tuff (Murature Fm.), trachydacite lavas and plugs (Ronald Fm.), trachydacite lava flows (Collins Fm.), basaltic andesite tephra cones and maars (Chacao Fm.), basaltic andesite tephra cones with craters (Casco Fm.), basaltic lavas and tephra (Kirkwood Fm.), and the modern andesitic tephra cones ad lavas of the Telefon Bay (Telefon Fm.).

Interpretation of our seismic profiles indicates that the submarine volcanic sediments can be arranged into several tectonostratigraphic units, which are separated by tectonically enhanced unconformities (Figs. 3 and 4). Each unconformity is interpreted in terms of deformation events that disturb the geometry of the sedimentary materials. Three major tectonostratigraphic units (A, B, and C) and seven subunits (B1–B5, C1, and C2) were distinguished. Unit A constitutes the basal unit (see Figs. 3 and 4) and shows transparent acoustic facies that can be correlated with the precaldera subaerial deposits before the collapse of DI caldera. Unit B is a syntectonic unit that is synchronous with the more significant volcanic and tectonic events. Subunits B1–B5 (Figs. 3 and 4) are clearly separated by progressive unconformities and host three main types of volcanic structures: mounds, submarine cones, and upward fluid vents.

The mound-type structures are located at the base of the unconformities between the B3, B4, and B5 subunits (Figs. 3 and 4), and they migrate upwards and laterally, increasing their size (up to 15 m in height) (Fig. 4). Disturbing of the successive even-stratified facies beneath the mounds could be due to injection vents that would act as feeders of the system. We interpret the mounds as hydrothermal processes bearing volcanic structures in a subma-

Table 1 Proposed correlations between subaerial volcanic events (Birkenmajer 1992) and tectonostratigraphic units defined by seismic profiles carried out in the flooded caldera of DI

Subaerial volcanic events (Birkenmajer, 1992)		Tectonostratigraphic units (this paper)		
Type and morphologies	Formation	Acoustic facies and structures	Unit	Type of deformation
Andesitic tephra cones and lavas, 1967–1970 volcanic events	Telefon	Even-stratified	C	—
Basaltic lavas and tephra, 1829–1912 volcanic events	Kirkwood	Even-stratified and slump chaotic facies	C	—
Basaltic andesite tephra cones with craters	Casco	Mound-type structures Fluid vent structures	B5	Bent Normal faults
Basaltic andesite tephra cones and maars	Chacao	Mound-type structures, submarine cones	B4	Tilted and bent
Trachydacite lava flows	Collins	Mound-type structures	B3	Tilted and bent
Trachydacite lava and plug	Ronald	Disturbed and chaotic facies	B2	Tilted and bent
Andesitic lapilli tuff	Murature	Distributed and chaotic facies	B1	Tilted and bent
Precaldera deposits	Foster Group	Transparent facies, unclear register	A	—

rine setting, which resemble the Fe–Mn mounds that have been described in other volcanic mineralized areas [e.g., Galapagos mound area, Corliss et al. (1978); Robertson and Boyle (1983)].

The volcanic cones outcrop on the sea-floor (Fig. 4) and give rise to large volcanic edifices that stand up from the sea-floor substrate up to 50 m (Fig. 4). The cone-shape morphology could be due to both a fast injection of magma and a rapid cooling caused by the extremely low temperatures of the seawater.

The existence of fluid vent structures is inferred from the partial masking of the reflector signals. Upward movement of the fluids is revealed by the deformation of the original disposition of the sea-floor and sub-sea-floor volcanic sediments (Fig. 3).

Finally, Unit C caps the trough formed by the bending of the underlying A and B units (Figs. 3 and 4). Subunits C1 and C2 are mainly composed of chaotic acoustic facies that can be interpreted as slumping deposits and even-stratified facies (sometimes disturbed by the vents at the top of the sequence).

A comparison between subaerial and submarine vol-

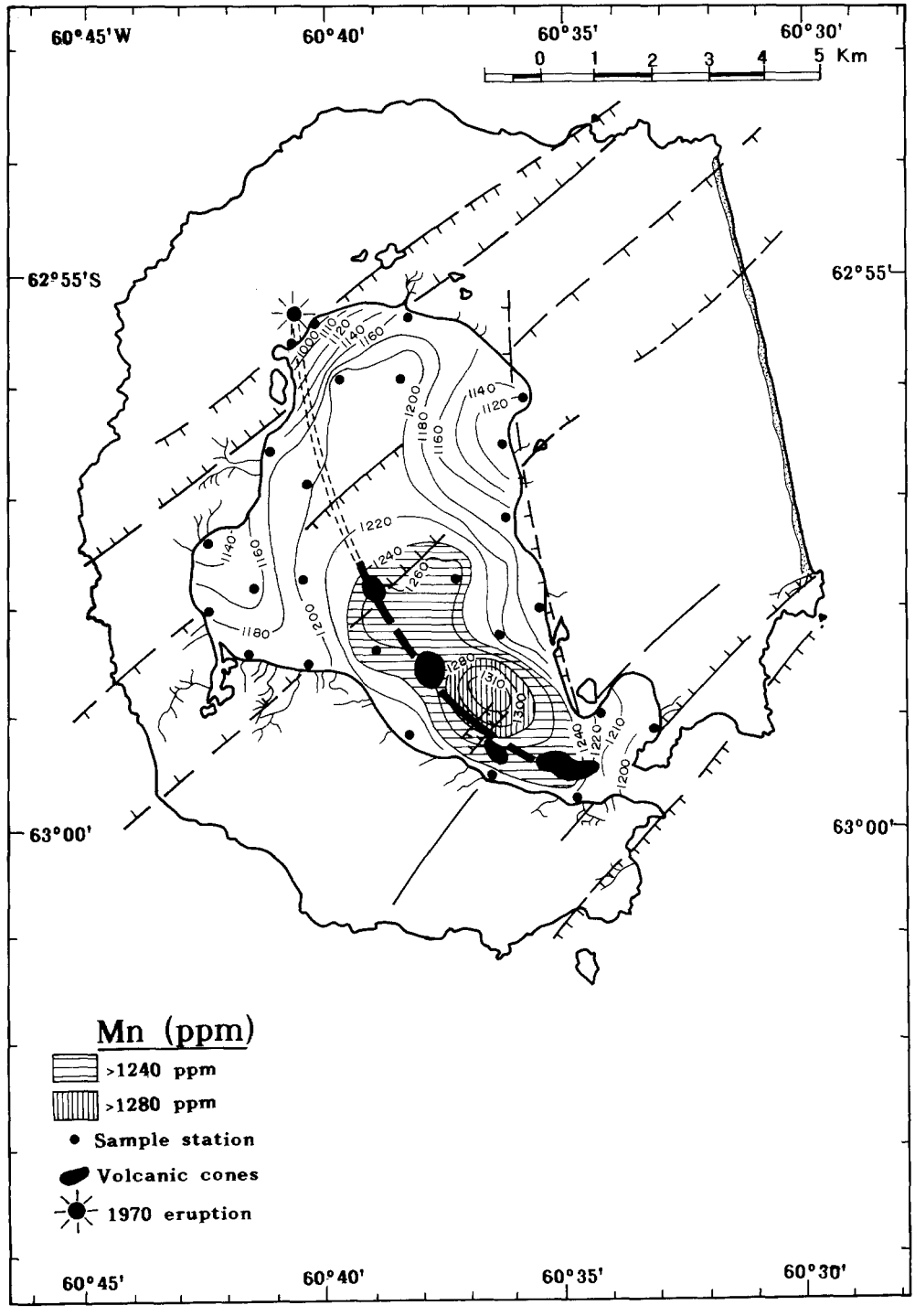

Fig. 5 Geochemical distribution pattern of Mn (ppm), which displays the highest values clearly related to the submarine volcanic cones and mounds (see Fig. 2)

canic events can be made on the basis of the relationship between subaerial syncaldera and postcaldera groups (Birkenmajer 1992) and synbending and postbending submarine units previously defined (see Table 1).

Geochemistry of volcanic and hydrothermal events

Recent geochemical analysis from sea-floor-dredged samples corresponding to the Quaternary volcanic sediments (Rey et al. 1993) demonstrate the existence of important chemical variations that could be the result of different submarine volcanic episodes. Thus, the sediment samples can be classified as: (1) metaluminous calc-alkaline according to their FeO–MgO–($Na_2O + K_2O$) relationship and $Al_2O_3/(CaO + Na_2O + K_2O)$ vs. $Al_2O_3/(Na_2O + K_2O)$ contents; (2) low potassium tholeiites, taking into account their log Cr/log Ti ratios, and (3) ocean floor basalts (OFB) in accordance with their Ti/100 vs. V relations.

Geochemical distribution patterns display the highest contents of Mn, Fe, and Zn coinciding with the position of the mounds and volcanic cones (Fig. 5). These values decrease progressively from the axis to the boundaries of the flooded caldera and the lowest values were detected at the Telefon Bay area. Thus, it is possible that the hydrothermal fluids linked to the syncaldera volcanic episode (unit B) would be richer in metals than those of the more recent eruptions (unit C).

The highest values of As, Al, Ca, Mg, and K are found between Fumarole Bay and Pendulum Cove, and coincide with the N60 axis that crosses the flooded caldera (Fig. 2). Currently active hydrothermal processes, such as fumaroles and hot springs, are associated with this axis in the areas of Fumarole Bay, Telefon Bay, Pendulum Cove, and Whalers Bay (Ortíz et al. 1987; Ramos et al. 1989). These authors propose that the fluids are produced by the venting of shallow aquifers heated by convective gaseous inflow from the underlying magma chamber. H_2 (0.010–0.066%), CH_4 (0.0010–0.066%), He (0.0010–0.019%), air, and water vapor are the main components (Ortíz et al. 1987) of fluids from the fumarole emissions.

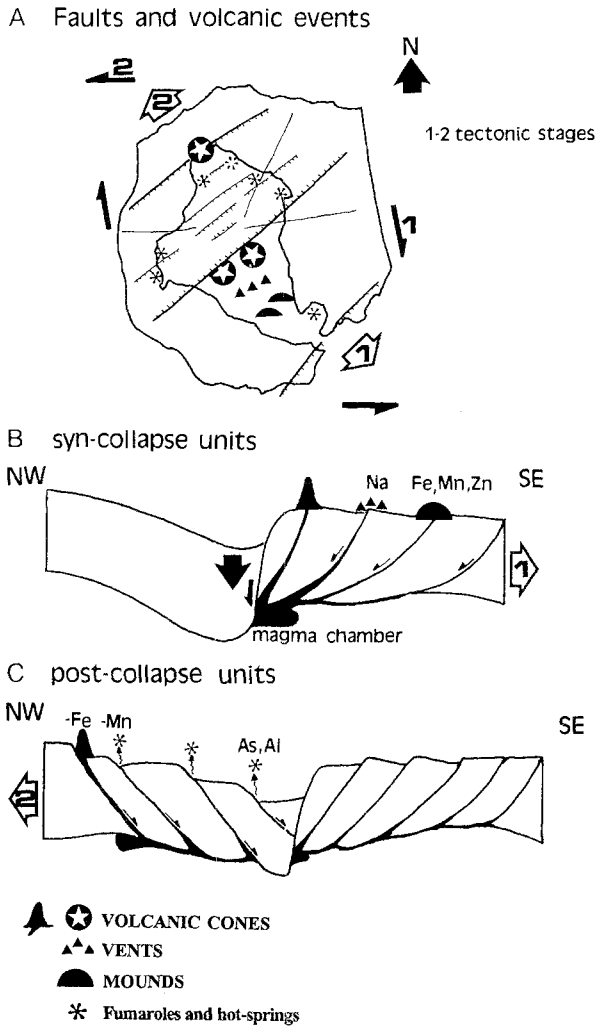

Fig. 6 A Relationship between the fault system and volcanic events. The volcanic events of the syncollapse units are caused by an asymmetric extension axis pulling toward the SE (stage 1) that gives rise to a major bend structure. Extension strengths are related to a pair of N170 right-lateral strike-slip faults (1) bordering the DI. Recent volcanic events of Telefon Bay (postcollapse units) and fumaroles are related to normal faulting caused by an asymmetric extension axis pulling toward the NW (stage 2). Extension strengths would be caused by an E–W left-lateral slip fault (2). **B** Interpretative cross section along a NW–SE axis of DI showing extension stage 1 with the volcanic structures (highest Fe, Mn, and Zn values) associated with the syncollapse units. **C** Interpretative cross section of stage 2 with normal faulting related with fumarole zones (highest As values) and recent volcanic processes (Fe- and Mn-deficient zones)

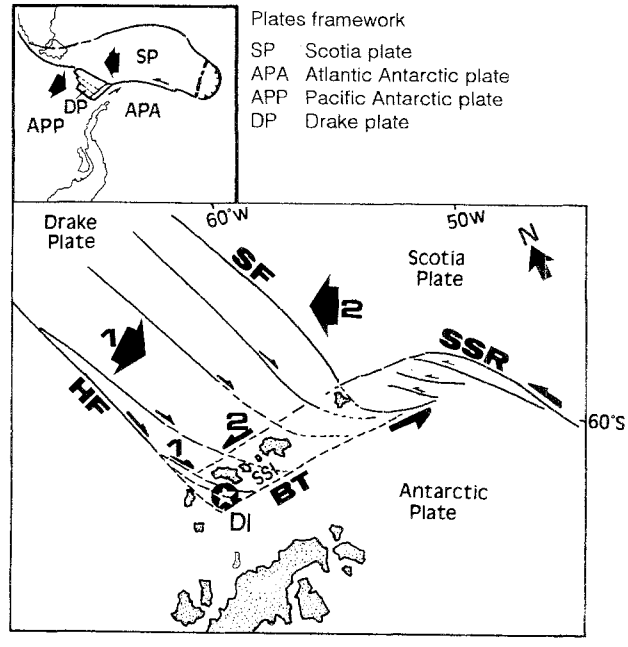

Fig. 7 A proposed regional tectonic model to explain the extension strain of DI caused by a pair of right (stage 1) and left (stage 2) lateral strike-slip faults. 1: southeast movement of the Drake Plate through the dextral fracture zone of Hero (HF) that affects DI. 2: movement of the Scotia plate westward through the South Scotia Ridge (SSR) generating a great left-lateral simple shear zone to the north of the Brandsfield Trough (BT). SF: Shackleton Fracture, SSI: South Shetland Islands.

Discussion and proposal of a model

Based on the correlation between tectonostratigraphic units, volcanic events, and geochemical distribution patterns of the sea-floor sediments, we propose that the DI flooded caldera was produced by a continuous extension process instead of by a "catastrophic-event" due to simple collapse of the caldera. The extension strike is generated as a consequence of a lateral simple shear stress around DI.

The first extension stage (Fig. 6B) is related to N170 right-lateral strike slip faults, one of which, the Macaroni fault, shaped the west side of the island. This right-lateral simple shear produced an extension strain along the NW–SE main axis of DI, causing progressive bending and N60 tension faults (SE side of DI). The main strain zone is located, therefore, in the center of DI, generating a major bend structure that gives rise to an upward movement of the magma chamber through low-angle tension faults. Bend and tilt events are responsible for progressive unconformities that separate the B tectonostratigraphic subunits. Each event is related to a sequence of volcanic structures and deposits (submarine volcanic cones, mounds, and fluid vent structures), which display high contents of Fe, Mn, and Zn. This stage would correspond to the syncollapse event.

A second extension stage produced normal faults, mainly on the northwest side of the DI, which are related to recent Telefon Bay volcanic events (with lower contents of Mn, Fe and Zn) and to the As-rich fumaroles and hot-spring areas. The fact that the strain mainly affects the northwest side of the island could mean that the maximum strain is caused by a left-lateral strike-slip just on the north of DI (Fig. 6C).

Therefore, the first extension stage would take place by pulling of the southeast corner of DI, mainly conditioned by a movement of a right-lateral strike-slip fault (Macaroni fault) and the second stage by pulling of the northwest corner by a movement of a pair of left-lateral strike-slip faults located on the north and south of DI (Fig. 6).

Thus, in a regional framework (Fig. 7), we propose that these two major lateral simple-shear zones around DI are the result of two different relative movements of plates that are consecutive in time: first, a southeastward movement of the Drake Plate onto the Antarctic Plate through right lateral strike-slip faults from the major Hero fracture (HER), second, the westward movement of the Scotia Plate, which affected the Drake Plate. This caused a regional left-lateral simple shear zone affecting the South Shetland Islands and Brandsfield Trough (Fig. 7).

Acknowledgments We would like to thank the members of the Antarctic Spanish Expedition (Oceanographic Vessel *Las Palmas*) for their collaboration, especially the expedition chief, Enrique Moreu. Thanks also to IEO (Instituto Español de Oceanografía) and CSIC (Consejo Superior de Investigaciones Científicas) for financial support of part of the research. This work has been carried out in cooperation with the IGCP project 318 (IUGS/UNESCO), and with the Spanish Working Group on Geology and Metallogeny of Seafloor Hydrothermal Deposits. Special thanks to Mathew Harffy for his critical review of the English version.

References

Barker PE, Pihil D, Macreath I, Harvey MR, Roobol MJ, and Davies TG (1975) The geology of the South Shetland Islands: V. The volcanic evolution of Deception Island. British Antarctic Survey Science Reports pp 78–81

Barker WA (1982) The Cenozoic subduction history of the Pacific margin off the Antarctic Peninsula: Ridge crest–trench interactions. Journal of the Geological Society of London 139:787–801

Birkenmajer K (1992) Volcanic sucession at Deception Island, West Antarctica: A revised lithostratigraphic standard. Studia Geologica Polonica 101:27–82

Corliss JB, Lyle M, Dymond DJ, and Crane M (1978) The chemistry of hydrothermal mounds near the Galapagos rift. Earth Planetary Science Letter 40:12–24

González-Ferrán O (1985) Volcanic and tectonic evolution of the Northern Antarctic Peninsula-Late Cenozoic to Recent. Tectonophysics 114:389–409

Grad M, Guterch A, and Sroda P (1992) Upper crustal structure of Deception Island area, Bransfield Strait, West Antarctica. Antarctic Science 4(4):469–476

Hawkes DD (1962) The structure of the Scotia Arc. Geological Magazine 99:85–91

Ortiz R, Valentín A, and Grimalt J (1987) Actividad fumaroliana en Decepción. Estudio preliminar. II Simposio Español de Estudios Antárticos, CSIC, Madrid pp 229–237

Ramos M, Ortíz, Díez-Gil JL, and Viramonte J (1989) Anomalías térmicas y balance de flujo energético sobre el suelo del volcán Decepción, Isla Decepción (Shetland del Sur). Actas del Tercer Simposium Español de Estudios Antárticos. Comisión Interministerial de Ciencia y Tecnología pp 203–219

Rey J, De Andrés JR, and Fernández-López JM (1990) Tectónica reciente en los depósitos submarinos de la bahía de Decepción. Actas del Tercer Simposium Español de Estudios Antárticos. Comisión Interministerial de Ciencia y Technología pp 258–270

Rey J, Somoza L, Martínez-Frías J, Del Barrio S, and Benito R (1993) Caracterización geoquímica de los sedimentos volcánicos submarinos de la Isla Decepción, Antártida. I Reunión Científica del Grupo de Trabajo "Geología y Metalogenia de Depósitos Hidrotermales Submarinos." I:4–5 (abstract)

Robertson AHF and Boyle JF (1983) Tectonic setting and origin of metalliferous sediments in the Mesozoic Tethis sediment. In: Rona PA, Borstrom K, Lambier L, and Smith KL (Eds.) Plenum Press New York & London, Hydrothermal Process at Seafloor Spreading Centers. NATO Conference Series, Vol 12, 796 pp

Smellie JL (1988) Recent observations on the volcanic history of Deception Island, South Shetland Islands. British Antarctic Survey Bulletin 81:83–85